RESEARCH PAPER

PCCP
www.rsc.org/pccp

Reactivity of cobalt dimer and molecular oxygen in rare gas matrices. IR spectrum, photophysics and structure of Co_2O_2

Delphine Danset and Laurent Manceron*

LADIR/Spectrochimie Moléculaire CNRS UMR 7075–Université Pierre et Marie Curie, case 49, 4 place Jussieu, 75252 Paris, France. E-mail: lm@ccr.jussieu.fr

Received 5th October 2004, Accepted 7th January 2005
First published as an Advance Article on the web 24th January 2005

The reactivity of cobalt dimer towards molecular oxygen has been investigated in rare gas matrices. If the formation of Co_2O_2 from the condensation of effusive beams of Co and O_2 in neon and argon matrices is observed after sample deposition, our results show that the *in situ* formation does not result from the reaction of ground state Co nor Co_2 with molecular oxygen. One reaction channel has been evidenced through reaction of Co_2 in excited states, close or above the dissociation limit. Two metastable states of Co_2O_2 with low-symmetry structures, stabilized by interaction with the matrix cage have also been evidenced between 1.4 and 2 eV above the ground state. Observation of $Co_2{}^{16}O_2$, $Co_2{}^{18}O_2$ and $Co_2{}^{16}O^{18}O$ isotopic data for five fundamental and three combination transitions enable determination of all fundamental vibrations for matrix-isolated Co_2O_2 in its cyclic ground state. Semi-empirical harmonic potential calculations lead to estimates of 2.435 N cm^{-1} for the Co–O bond force constant, and 93 ± 5° OCoO bond angle. In comparison with the CoO diatomic molecule, this suggests a near square-planar structure with a 1.765 ± 0.01 Å CoO bond distance.

Introduction

Cobalt oxides, usually supported on silica or alumina, are used in catalysis[1,2] and some studies have investigated the adsorption of small molecules on the active sites of cobalt oxides. For instance, Co_2O_2 local defects seem to be active sites in methanol chemisorption processes, as well as other small molecules on bulk CoO or Co_3O_4 surfaces.[3,4] However, studies on such systems at the molecular scale are scarce. Gas phase studies on well-defined cobalt oxide systems, other than the diatomic molecule, are restricted to mass spectroscopic studies investigating the reactivity and kinetics for chemisorption and dissociation processes on small cationic cobalt molecules and clusters.[5–7] $Co_2O_2{}^+$ cationic species have been formed in sequential reactions involving $Co_2{}^+$ in an ion trap and were reported to have a particular stability,[6] which stimulated theoretical studies on Co_2NO^+ and $Co_2O_2{}^+$ species.[8] For neutral dicobalt oxide molecules no structural data are, to our knowledge, yet available in the gas phase. Chertihin *et al.*[9] studied the reaction products of laser-ablated cobalt atoms and molecular oxygen isolated in solid argon and identified Co_2O_2 as a rhombic, D_{2h} symmetry molecule through two of its fundamental vibrations, corresponding to in-plane ring stretching modes. DFT calculations were performed for several states of different spin multiplicities (^7A_u, $^5B_{3u}$ and $^5B_{1g}$). The septet state was found to be lower in energy, by 7 and 27 kcal mol^{-1} than the $^5B_{3u}$ and $^5B_{1g}$ states, respectively. Frequencies were calculated and compared to the existing experimental data, but the comparison was not conclusive. No calculation for singlet or triplet states has yet been reported. In comparison with alkali metal peroxides of M_2O_2 stoichiometry, the structure seems to differ as the O–O linkage seems broken, with a stronger metal–oxygen interaction due to the 3d orbitals of the transition metals.

In light of the large differences in reactivity, which are often encountered between atoms and small metal clusters, it seems interesting to compare the Co + O_2 and Co_2 + O_2 reactions using low-energy thermally evaporated cobalt, as both Co and Co_2 present numerous low-lying excited states.[10,11]

In this study, we present new information concerning the formation of Co_2O_2 in the conditions of matrix isolation in solid argon and neon at low temperature. Since large quantities of this molecule could be isolated, new vibrational data have been obtained, which bring structural information. Also new data concerning two metastable states have been obtained and are briefly discussed.

Experimental

The experimental set-up has been described previously.[11,12] Briefly, Co_2O_2 molecules were formed by co-condensing Co vapor and dilute O_2–Ar or Ne mixtures, onto one of six flat, highly polished, Rh-plated copper mirrors maintained between 3 and 30 K using a pulse-tube, closed-cycle cryogenerator (Cryomech PT405, USA). The system was evacuated at a base pressure of about 7.10^{-8} mbar before refrigeration of the sample holder. The metal atom flux from a resistively heated Co-wetted W filament was carefully monitored with a quartz microbalance and was varied from 1 to 10 nanomol min^{-1}. For most samples, this corresponded to 50 to 500 ppm Co/Ne and 200 to 2000 ppm Co/Ar molar ratios.

High purity Argon and Neon (Air Liquide, France; 99 995% and 999 995%), $^{16}O_2$ (Air Liquide, France; 99 998%) and $^{18}O_2$ (Isotec, USA, 99.0% ^{18}O), were used to prepare the O_2–Ar/Ne mixtures. Scrambled oxygen ($^{16}O_2$,$^{16}O^{18}O$, $^{18}O_2$), was prepared by mixing equal quantities of $^{16}O_2$ and $^{18}O_2$ in a Tesla discharge. The gas inlet line was driven through the liquid nitrogen trap within the vacuum system thereby condensing some impurities in the mixture and precooling the gas to 77 K before attaining the mirror.

In general, after 15–90 min of deposition, absorption spectra were recorded between 30 000 and 50 cm^{-1} on the same samples using a Bruker 120 FT spectrometer with resolution varied between 0.05 and 1 cm^{-1}. Combinations of detectors/sources/beamsplitters are described in ref. 11. Bare mirror backgrounds, recorded prior to sample deposition, were used as references in processing the sample spectra. The spectra were subsequently subjected to baseline correction to compensate

DOI: 10.1039/b415420g

for infrared light scattering and interference patterns. Photo-excitations were performed through a CaF_2 window in two different ways. First, the efficient energy ranges were roughly defined using wide band sources (black bodies for NIR and 200 W HgXe arc lamp for UV-Vis regions) coupled to band pass filters, and focused on the sample (surface ≈ 1 cm^2). Typically, photo-excitations in the NIR region with 40 mW cm^{-2} were routinely achieved using a 9500–6000 cm^{-1} bandpass filter in combination with a 150 W globar source, and lasted up 10 to 30 min. It quickly appeared that both reactants and products had electronic absorptions in the same energy ranges, and more monochromatic excitations were needed to characterize specific processes. Selective excitations were first performed in the visible and UV ranges using narrow (10 nm fwhm) bandpass interference filters. Irradiances were measured with an optical power meter, and were of the order of 7, 18 and 14 mW for 10 nm bands centered at 405, 435 and 546 nm, respectively. Narrow band photoexcitations (5 to 6 cm^{-1} line width) were also performed over a wider range using the idler beam of an OPO source operating with a BBO crystal, pumped by the third harmonics of a Nd-YAG Laser (OPOTEK, QUANTEL), delivering ≈ 0.5 mJ at 20 Hz, continuously tunable in the 25 000–4300 cm^{-1} range.

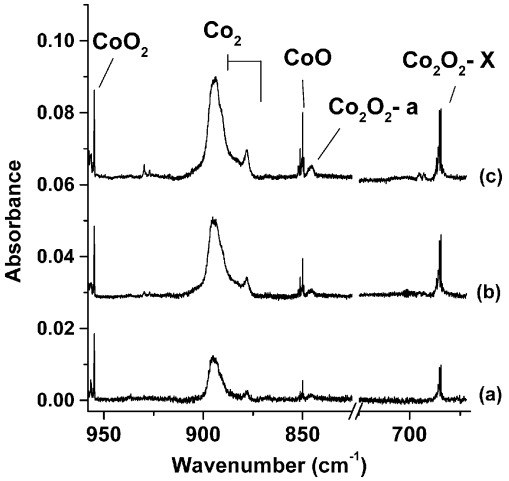

Fig. 1 A concentration study of the Co, $Co_2 + O_2$ reaction in solid Ne: IR absorption spectra in the 960–650 cm^{-1} region for three different samples deposited at ≈ 4.8 K with O_2/Ne = 500 ppm. Normalization factors are applied to obtain equal intensities on the known CoO_2 ν_3 absorption. (a) Co/Ne $\approx$ 30 ppm, absorbance $\times$ 1, (b) Co/Ne $\approx$ 100 ppm, absorbance $\times$ 0.71, (c) Co/Ne $\approx$ 250 ppm, absorbance $\times$ 0.5.

Results

Samples were grown co-depositing thermally evaporated Co atoms with very dilute O_2/Ne mixtures, in order to keep at a negligible level the oxide species containing more than one oxygen molecule which have been previously identified, such as CoO_4 and Co_2O_4.[9,13] Typically, the O_2/Ne molar ratio was varied from 200–2000 ppm and the Co/Ne in the 50–500 ppm range, over more than twenty different samples.

As observed previously, only small amounts of CoO_2 molecules are formed in the absence of electronic excitation of atomic Co,[13] absorption bands belonging to other species can also be observed in the mid-IR range. These absorptions belong to cobalt dimer, Co_2, and to CoO. Co_2 can be traced in the mid infrared range by several vibronic progressions, previously characterized, with the strongest features corresponding to the (0,0) B–X and C–X bands near 900 and 2863 cm^{-1}, respectively.[11] Formation of the CoO diatomic molecule can also be followed by its vibrational fundamental near 851 cm^{-1}, and electronic transitions with origins near 3377 and 5808 cm^{-1} and associated vibrational structures[12] (Figs. 1–3). In addition, two absorption centered at 685.2 and 467.1 cm^{-1} (labeled Co_2O_2–X) were prominent and very close to those assigned to rhombic Co_2O_2 by Chertihin *et al.*[9] in argon, at 685.2 and 469.6 cm^{-1}. Experiments performed by varying the Co/Ne and O_2/Ne molar ratios, confirmed the second order dependence in Co and first order in O_2 for this species, with a growth rate parallel to that of the Co_2 transitions, when increasing the metal concentration (Fig. 1). Two other, broader absorptions near 847 and 545 cm^{-1} were also detected with a parallel behaviour. Experiments repeated in argon confirmed the bands detected by Chertihin *et al.* and led to the observation of additional ones, which will be discussed below, but formation of CoO was not detected in these experiments (Table 1). In the experiments run in neon, it appeared that the CoO bands grew strongly with Co concentration, similar to Co_2, but also that other factors were influencing the CoO and Co_2O_2 relative product yields (Figs. 1 and 2). In particular, the relative product yields were very sensitive to the sample deposition temperature. When samples were deposited at the lowest achievable temperature with our system (about 2.8 K, Fig. 2a), the overall product yield was low and samples contained small amounts of Co_2, Co_2O_2, the two weak bands near 847 and 545 cm^{-1} (labeled Co_2O_2–a) and CoO was barely detectable. With a higher deposition temperature (about 4.8 K, Fig. 2b) to increase diffusion during the neon freezing process, the overall Co_2 and Co_2O_2 yield was about three times larger, while CoO increased by almost one order of magnitude. Increasing further the temperature above 6 K led to the disappearance of Co_2 and a relative decrease of Co_2O_2 and CoO at the benefit of larger oxide species, such as CoO_4 and Co_2O_4.[9,13] Annealing the sample after deposition up to 11 K had a completely different result (Fig. 3). This promoted formation of some larger species by molecular diffusion but did not affect the Co_2O_2/CoO relative yields, once the products were trapped and relaxed in their ground electronic state. Once formed, the CoO molecules proved to be quite unreactive, decreasing only slightly after annealing and molecular diffusion, but no dimerization was evidenced. Likewise, annealing effects prior to photoexcitations did not lead to noticeable increase in Co_2O_2–X at the expense of Co_2 or CoO.

As every possible precursor of Co_2O_2 is known to present electronic transitions to access low-lying electronic states in the UV–visible range, photoexcitations were tested systematically over the 0.2–5 eV range,[11,14–17] and effects have been observed in different energy ranges. More insight on the Co_2O_2–X formation can be gained from these effects, but they need to be analyzed in some detail, as excitations in the same domain

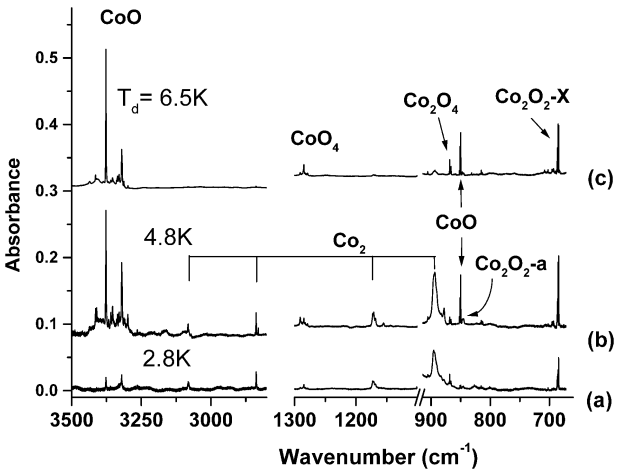

Fig. 2 Effects of the deposition temperature (T_D) on the relative yields of the Co, $Co_2 + O_2$ reaction products. IR absorption spectra on three samples deposited with about the same Co/O_2/Ne = 0.25/0.5/1000, but three different deposition temperatures.

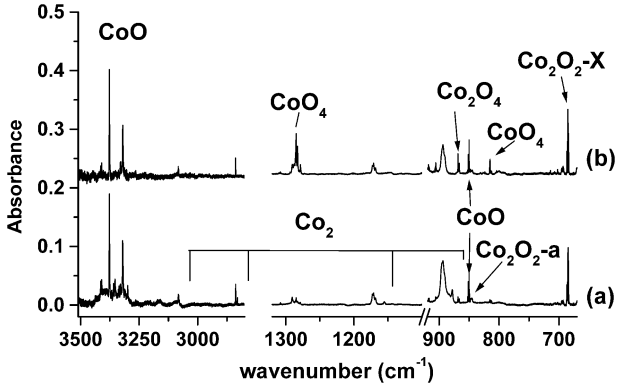

Fig. 3 Effects of sample annealing temperature on the relative yields of the Co, $Co_2 + O_2$ reaction products. IR absorption spectra for a $Co/O_2/Ne = 0.25/0.75/1000$ sample. (a) After deposition at ≈4.5 K, (b) after cycling the temperature at ≈11 K and back to ≈4.5 K.

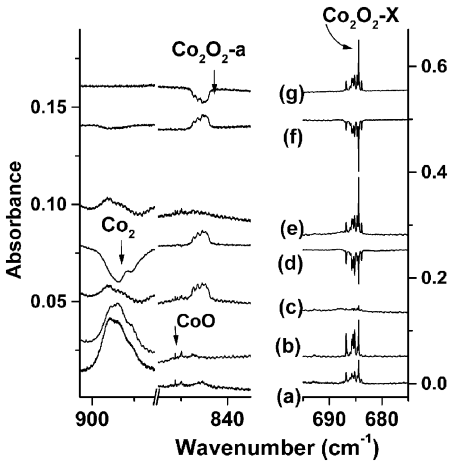

Fig. 4 Effects of various photoexcitations on the different $Co_2 + O_2$ reaction products observed in solid neon. IR absorption spectra for a sample deposited with $Co/O_2/Ne = 0.2/0.5/1000$, (a) after deposition at 3 K, (b) after broad band 9500–6000 cm^{-1} excitation, (c) after 17 500–17 000 cm^{-1} excitation, (d) difference spectrum (c) − (b), (e) spectrum after a second broad band 9500–6000 cm^{-1} excitation, as in (b), (f) difference spectrum after minus before another excitation at 18 310 cm^{-1}, (g) difference spectrum displaying the effect of a third photoexcitation around 8000 cm^{-1}.

can lead to different results, depending on sample history and variations in precursor populations. Fig. 4 displays such a sequence, starting from observation of a dilute sample ($Co/O_2/Ne = 0.2/0.5/1000$) containing only small quantities of Co_2, CoO, Co_2O_2–X and Co_2O_2–a products (trace 4a). It appears that photoexcitation in the near IR between 9000 and 6000 cm^{-1} induces an increase of the 685 cm^{-1} band (small growth of the Co_2O_2–X species), at the expense of the Co_2O_2–a species (disappearance of the 847 cm^{-1} band, trace 4b). Next, two species appear photosensitive in the visible range (between 540 and 600 nm), the Co_2 species and Co_2O_2–X (trace 4c). Both are strongly decreased by irradiation in this wavelength range, and a marked growth of the Co_2O_2–a band near 847 cm^{-1} can be correlated, best observed on the difference spectrum (trace 4d). Note that Co_2 was shown previously to present electronic absorptions in this range but, in absence of oxygen in the sample, excitation in this range led only to small changes in band profiles, not to disappearance of the Co_2 molecules.[11] Excitations at lower energies corresponding to Co_2 vibronic transitions did not produce noticeable effects. Next, a second photoexcitation in the 9000–6000 cm^{-1} range, identical to that performed in the second step reformed the absorption correlated to species Co_2O_2–X, at the expense of those of species Co_2O_2–a (trace 4e). From there on, conversion between these two forms could be repeated many times on the same sample, switching to the cyclic form following photoexcitations with near IR cm^{-1} and reverting to the new Co_2O_2–a form with visible light (see traces 4f and 4g). Attempts were made to observe the electronic absorptions corresponding to these transitions, but due to overlapping with strong absorption bands of CoO around 545 nm[12,17] on the one hand, and to the extreme sensitivity of Co_2O_2–a in the near IR range on the other, no unambiguous observation could be made. Experiments using narrow range photoexcitation with the OPO source showed a fairly broad excitation profile with an approximately equal yield between 9000 and 6000 cm^{-1} for Co_2O_2–a to Co_2O_2–X conversion, with a decreasing efficiency in the 9500–9000 and 6000–5500 cm^{-1} ranges. It is thus likely that the efficient electronic absorption of Co_2O_2–a is broad and structureless.

Once all Co_2 molecules have reacted, the photoconversion between the different forms of Co_2O_2 can be repeated at will and selectively. This constitutes a powerful means for confirming the correlation of very weak bands to the main absorptions of Co_2O_2–X (see Fig. 5 for the weak band observed near 917 cm^{-1} in Ne). Experiments were repeated with $^{18}O_2$, $^{16}O_2 + {}^{18}O_2$ and $^{16}O_2 + {}^{16}O^{18}O + {}^{18}O_2$ mixtures to obtain isotopic effects for all species in both neon and argon matrices and isotopic data are listed in Tables 1 and 2. Care was taken to

Table 1 Frequencies for observed IR absorptions (cm^{-1}) for $Co_2 + O_2$ reaction products in solid Ar

$^{16}O_2$	$^{18}O_2$	$^{16}O^{18}O$[a]	Assignment
1393.2 (0.002)[b]	1325.6	—	Co_2O_2–X ($\nu_1 + \nu_6$)
985.5	931.0	959, 947	Co_2O_2–b
950.2	907.5	943.5, 913.9	Co_2O_2–b
929.6 (0.038)	890.7	899.9	Co_2O_2–X ($\nu_3 + \nu_5$)
862.2 (0.069)	827.2	836.4	Co_2O_2–X ($\nu_2 + \nu_6$)
839.4	805.0	838.6, 806.6	Co_2O_2–a
—	—	703.1 (0.29)	Co_2O_2–X (ν_1)
685.2 (1.00)	655.1	661.1 (1.00)	Co_2O_2–X (ν_6)
551.5	531.8	550.0, 533.6	Co_2O_2–b
544.8	519.1	543.0, 521.3	Co_2O_2–a
530.0	505.7	528.3, 507.8	Co_2O_2–a
469.5 (0.57)	449.1	465.9 (0.60)	Co_2O_2–X (ν_5)
—	—	445.3 (0.22)	Co_2O_2–X (ν_3)
304.1 (0.17)	290.9	297.6 (0.25)	Co_2O_2–X (ν_4)
140.8	135.0	139.6, 136.3	Co_2O_2–a

[a] Additional absorptions observed in a $^{16}O_2 + {}^{16}O^{18}O + {}^{18}O_2$ mixture. [b] IR intensities relative to the strongest fundamental (±20% uncertainty).

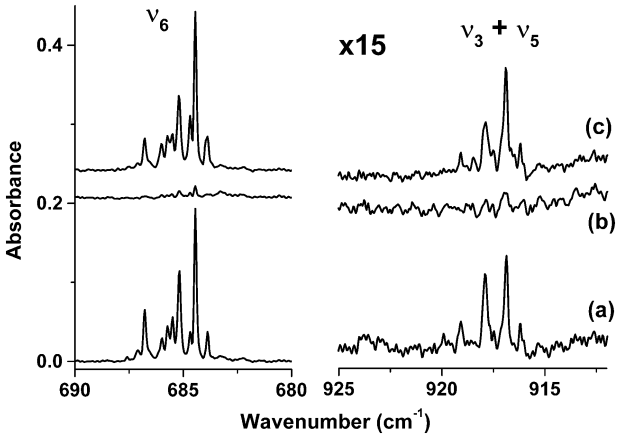

Fig. 5 Photoexcitation effects observed for $Co_2{}^{16}O_2$ in solid neon in the ν_6 and $\nu_3 + \nu_5$ regions. (a) After deposition, (b) after 546 nm, (c) after broad band 9500–6000 cm^{-1} excitation.

Table 2 Observed frequencies (cm^{-1}) for $Co_2 + O_2$ reaction products in solid Ne

$^{16}O_2$	$^{18}O_2$	$^{16}O^{18}O$[a]	Assignment
5755.4/**5808.2**[bc]	5757.2/**5809.8**	—	CoO A–X System
3320.2/**3376.7**	3321.0/**3377.6**	—	CoO B–X System
849.9/**851.2**	812.3/**813.5**	—	CoO
916.87 (0.03)	**879.15**	**899.89**	Co_2O_2–X ($\nu_3 + \nu_5$)
867.10 (0.05)	**832.25**	≈**841**[d]	Co_2O_2–X ($\nu_2 + \nu_6$)
847.2	810.7	845.5, 812.5	Co_2O_2–a
—	—	702.20	Co_2O_2–X (ν_1)
684.46 (1.00)	**654.41**	**660.42**	Co_2O_2–X (ν_6)
≈545 (broad)	≈541, ≈524	≈520	Co_2O_2–a
467.15 (0.67)	**446.53**	**461.80**	Co_2O_2–X (ν_5)
—	—	437.69	Co_2O_2–X (ν_3)
293.38 (0.24)	**287.07**	**280.58**	Co_2O_2–X (ν_4)

[a] Additional absorptions observed in a $^{16}O_2 + {}^{16}O^{18}O + {}^{18}O_2$ mixture. [b] In bold: main trapping site of a multiplet. [c] See ref. 12. [d] Tentative, very weak.

perform experiments with $^{16}O_2 + {}^{18}O_2$ mixtures, but these yielded the same frequencies as obtained with either $^{16}O_2$ or $^{18}O_2$ alone, as expected for species containing only two O atoms from the same O_2 molecule, and are not reported in Tables 1 and 2. When comparing data obtained in solid argon and neon, in addition to the usual and relatively small frequency shifts, minor changes in band profiles were observed for the Co_2O_2–X species. In neon, when observing at higher resolution (≤ 0.1 cm^{-1}) all absorptions are split into a tight multiplet of sharp absorptions (fwhm ≈ 0.2 cm^{-1}) whose intensity patterns differ slightly from one fundamental to the next and between the symmetrical isotopomers ($Co_2{}^{16}O_2$, $Co_2{}^{18}O_2$) and the other ($Co_2{}^{16}O^{18}O$). This latter effect is due to inhomogeneous crystal environment (the site multiplicity can be reduced by prolonged annealing above 11 K) but will be useful later to discuss vibrational assignments. More importantly, a large difference appears when comparing the effects of the same electronic excitation of the Co_2O_2–X species in either argon or neon. In solid neon, only one set of bands appears (847 and 545 cm^{-1}, labeled Co_2O_2–a) following 546 nm excitation. In argon, the corresponding bands appear slightly shifted (near 839, 545 and a supplementary weak signal near 141 cm^{-1}) but also, three supplementary absorptions appear for which no equivalent is found in the neon samples (near 985, 950 and 551 cm^{-1}). They are labeled Co_2O_2–b on the figures. Note that, when normalizing the intensities of disappearing Co_2O_2–X in neon and argon on the 685 cm^{-1} band, it appears that the relative intensities of the Co_2O_2–a group are about 20% smaller in argon than in neon. It therefore appears that the conversion process observed in neon and argon differ by the stabilization of at least one supplementary state:

$$\text{In neon}: Co_2O_2 - X \underset{\lambda=1100-1800\,nm}{\overset{\lambda=590-540\,nm}{\rightleftarrows}} Co_2O_2 - a$$

$$\text{In neon}: Co_2O_2 - X \underset{\lambda=1100-1800\,nm}{\overset{\lambda=590-540\,nm}{\rightleftarrows}} \begin{matrix} Co_2O_2-a \\ + \\ Co_2O_2-b \end{matrix}$$

Some important points of the isotopic effects on the Co_2O_2–X, -a and -b states vibrational transitions are presented in Figs. 6–9. In neon, the new 293.4, 867.1 and 916.9 cm^{-1} bands of Co_2O_2–X were shifted by −12.8, −34.8 and −37.8 cm^{-1}, respectively, using $^{18}O_2$ and showed a doublet structure with ($^{16}O_2 + {}^{18}O_2$) mixtures and a triplet structure in the samples containing ($^{16}O_2 + {}^{16}O^{18}O + {}^{18}O_2$) precursors, showing a single $Co_2{}^{16}O^{18}O$–X counterpart (Fig. 7 and Table 2). In isotopic mixtures where $^{16}O^{18}O$ precursor was present, the bands near 685 and 469 cm^{-1} showed an asymmetric triplet structure, with $Co_2{}^{16}O^{18}O$–X components shifted to lower and upper frequency, respectively, away from the expected, intermediate position between the $Co_2{}^{16}O_2$–X and $Co_2{}^{18}O_2$–X positions. Simultaneously, weak bands appeared outside the $Co_2{}^{16}O_2$–X and $Co_2{}^{18}O_2$–X absorptions ranges, at 703.1 and 437.7 cm^{-1} (Figs. 6 and 7).

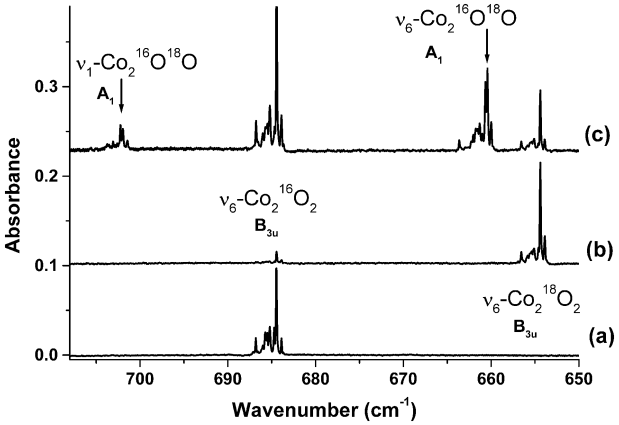

Fig. 6 IR absorption spectra in solid neon in the ν_1 and ν_6 regions for $Co_2{}^{16}O_2$, $Co_2{}^{18}O_2$, $Co_2{}^{16}O^{18}O$ isotopomers. $Co/O_2/Ne = 0.2/0.5/1000$, with (a) $^{16}O_2$, (b) $^{18}O_2$ and (c) $^{16}O_2/{}^{16}O^{18}O/{}^{18}O_2 \approx 0.35/0.48/0.17$.

The isotopic behaviors of the Co_2O_2–a and Co_2O_2–b absorptions are different. For Co_2O_2–a the upper fundamental near 840 cm^{-1} presents a $^{16}O_2/{}^{18}O_2$ shift of 34 cm^{-1} and a quartet pattern with $^{16}O_2 + {}^{16}O^{18}O + {}^{18}O_2$ mixtures, indicating additional bands for $Co_2{}^{18}O^{16}O$ and $Co_2{}^{16}O^{18}O$ isotopomers, shifted by about +1 and −1 cm^{-1} from the $Co_2{}^{16}O_2$ and $Co_2{}^{18}O_2$ positions. This is best observed in argon, where the absorptions are sharper than in neon (Fig. 8). Similar effects are observed on the other Co_2O_2–a absorptions near 545, 530 and 141 cm^{-1}.

The two upper bands observed for Co_2O_2–b have very different $^{16}O_2/{}^{18}O_2$ isotopic shifts, −54.5 cm^{-1} for the broad band near 985 cm^{-1} and −42.7 for the sharper band near 950 cm^{-1} (Fig. 9). The $^{16}O^{18}O$ counterparts are best evidenced by subtracting out the $Co_2{}^{16}O_2$ and $Co_2{}^{18}O_2$ bands in an experiment led with a $^{16}O_2 + {}^{16}O^{18}O + {}^{18}O_2$ mixture. Four bands are then detected, two broader ones at about 960 and 947 cm^{-1}, followed by two sharper ones at about 943.5 and 914 cm^{-1} (trace 9d). Additionally, a weaker band is observed near 552 cm^{-1}, which has no equivalent in the neon experiments where Co_2O_2–b is not formed, also presenting two isotopic counterparts with $^{16}O^{18}O$ precursor, and is tentatively assigned to this species, but the proximity with stronger bands makes this assignment less certain.

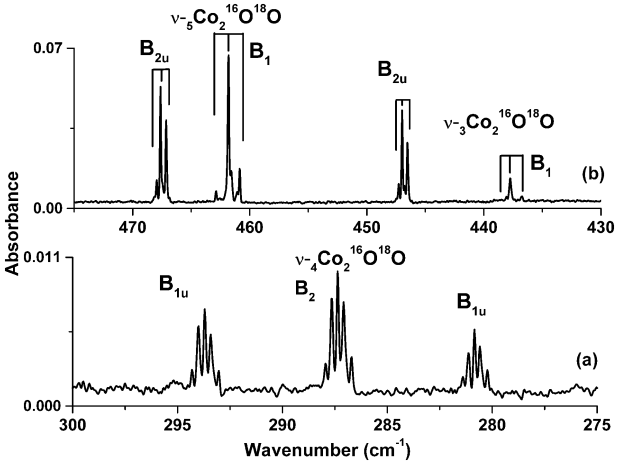

Fig. 7 IR absorption spectra in solid neon in the ν_4 (a), ν_3 and ν_5 (b) regions for $Co_2{}^{16}O_2$, $Co_2{}^{18}O_2$, $Co_2{}^{16}O^{18}O$ isotopomers. $Co/O_2/Ne = 0.2/0.5/1000$, with $^{16}O_2/{}^{16}O^{18}O/{}^{18}O_2 \approx 0.25/0.5/0.25$.

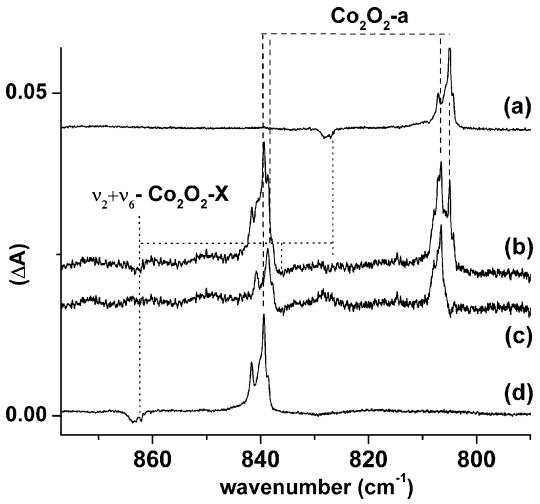

Fig. 8 Difference IR absorption spectra: after minus before 546 nm excitation on various Co_2O_2–b isotopomers in the 1000–900 cm^{-1} region in solid argon. The Co_2O_2–b bands appear as positive features, the weak negative feature (*) corresponds to the Co_2O_2–X $\nu_3 + \nu_5$ combination. (a) $Co_2{}^{18}O_2$, (b) $Co_2{}^{16}O_2 + Co_2{}^{16}O^{18}O + Co_2{}^{18}O_2$, (c) trace b—traces (a + d) to isolate $Co_2{}^{16}O^{18}O$ isotopomers, (d) $Co_2{}^{16}O_2$.

Discussion

The IR features observed from the $Co_2 + O_2$ reaction are shown to arise from the cyclic Co_2O_2–X molecule, two of its isomeric forms or metastable states, Co_2O_2–a and Co_2O_2–b, formed either directly or after electronic excitation, and diatomic CoO. Before studying the interplay of photophysical and chemical processes leading to the formation of each of these, the structural information that can be drawn from vibrational data will be examined.

Vibrational analysis and structure of Co_2O_2–X

A cyclic Co_2O_2 structure with a D_{2h} symmetry had been previously proposed through two IR-active Co–O stretching fundamentals[9] near 685 and 469 cm^{-1} in argon. New data having been obtained, completing the vibrational spectrum, this will enable a more precise structural discussion. Six IR bands now characterize this molecule in solid argon for the symmetrical isotopomers, along with two additional bands

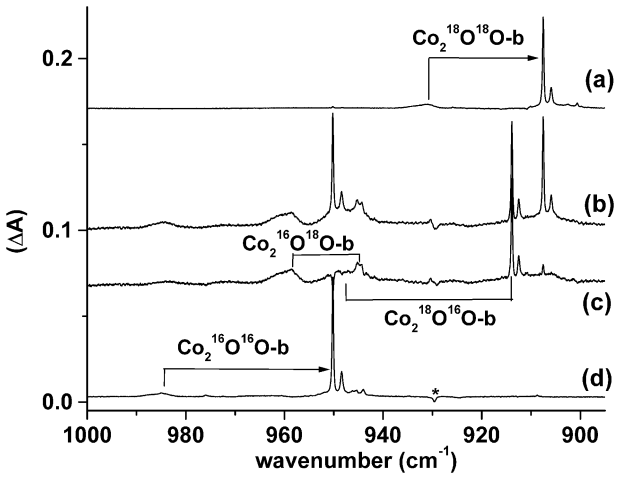

Fig. 9 Difference IR absorption spectra: after minus before 546 nm excitation on various Co_2O_2 isotopomers in the 880–780 cm^{-1} region. The Co_2O_2–a bands appear as positive features, the weak negative feature corresponds to the Co_2O_2–X $\nu_2 + \nu_6$ combination and the * designates a CoO_4 trace. (a) $Co_2{}^{18}O_2$ in argon, (b) $Co_2{}^{16}O_2 + Co_2{}^{16}O^{18}O + Co_2{}^{18}O_2$ in argon, (c) trace b—traces (a + d) to isolate $Co_2{}^{16}O^{18}O$ isotopomers, (d) $Co_2{}^{16}O_2$ in argon.

observed for the less symmetrical $Co_2{}^{16}O^{18}O$ isotopomer. In neon, as the absolute product yield was about three times weaker, the weakest band (above 1390 cm^{-1}) was not observed. All other counterparts are observed within 0.5% shifts, on average. The bands observed below 710 cm^{-1} are assigned to fundamental transitions, two orders of magnitude stronger than the three very weak bands above 860 cm^{-1}, thus assigned to combinations.

Several observations confirm the D_{2h} symmetry. In this hypothesis, a third IR-active fundamental is expected at lower frequency, corresponding to the out-of-plane deformation. It is observed here near 304 cm^{-1} and 293 cm^{-1} in argon and neon, respectively. The symmetrical triplet isotopic structure observed with $^{16}O_2 + {}^{16}O^{18}O + {}^{18}O_2$ mixtures shows that the two oxygens in the molecule are equivalent. Additionally, the IR-activation of absorption bands near 703 and 440 cm^{-1} with sizable intensities using $^{16}O^{18}O$ precursor indicates the loss of the inversion center (Fig. 7).

With a rhombic structure and D_{2h} symmetry, the six fundamental vibrations of $Co_2{}^{16}O_2$ span the representations $2A_g + B_{1g} + B_{1u} + B_{2u} + B_{3u}$, with only the latter three being IR-active. Specification of the reference axes is necessary to avoid ambiguities in vibrational assignments, therefore the choice of axes adopted hereafter is shown on Fig. 10, following Wilson's convention.[18] For the $Co_2{}^{16}O^{18}O$ molecule, the molecular symmetry is lowered to C_{2v} and with our choice of axes the representations span $3A_1 + 2B_1 + B_2$, all being formally IR-active. The out-of-plane deformation (of B_{1u} symmetry for the symmetrical species) is the only one remaining alone in its symmetry class, and correlate with B_2 in $Co_2{}^{16}O^{18}O$. This explains the symmetrical isotopic pattern observed for the lowest frequency fundamental (Fig. 7), as harmonic coupling with the other modes is not possible and the isotopic shifts result only from the steady variation in reduced mass. For the other, in-plane Co–O stretching modes, asymmetries in the positions of the $Co_2{}^{16}O^{18}O$ counterparts and activation of *gerade* modes near 710 and 460 cm^{-1} stem from the molecular symmetry reduction, as A_g and B_{3u} motions are now both of A_1 symmetry, and B_{1g} and B_{2u} both of B_1 symmetry. At this point assignment of the 685 and 469 cm^{-1} band to either B_{2u} or B_{3u} motions is possible, but unambiguous assignment will be proposed on the basis of two observations.

First, an estimation of the isotopic effects on the B_{1u}, B_{2u} or B_{3u} modes can be obtained using Wilson's formalism based following the variation of the reduced mass. With α being the OCoO, the inverse reduced masses for the B_{3u} Co–O stretching (ν_6) vibration of $Co_2{}^{16}O_2$ can be expressed on the basis of symmetry coordinates as $G_S(B_{3u}) = \mu_{Co}(1 + \cos\alpha) + \mu_O(1 - \cos\alpha)$. If ν_6 and ν'_6 relate to the fundamental frequencies of $Co_2{}^{16}O_2$ and $Co_2{}^{18}O_2$, the expected value of the isotopic ratio

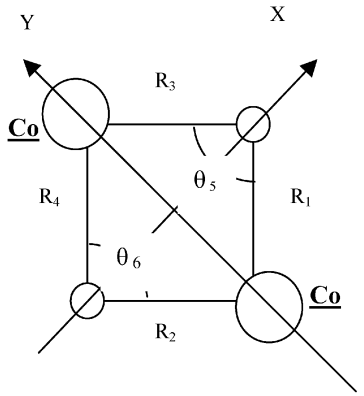

R_e= 1.765±0.01 Å

θ = 87° ± 5°

Fig. 10 Proposed structure for ground state Co_2O_2 –X and coordinate and axis definition for vibrational assignments.

will be:

$$\nu_6/\nu'_6 = (\mu_{Co}(1 + \cos\alpha) + \mu_O(1 - \cos\alpha)/\mu_{Co}(1 + \cos\alpha) + \mu_O(1 - \cos\alpha))^{1/2} \quad (1)$$

For the B_{2u} mode, the corresponding will be G_S (B_{2u}) = $\mu_{Co}(1 + \cos\alpha) + \mu_O(1 + \cos\alpha)$. Thus the value of the isotopic ratio expected for ν_5 will be independent of the bond angle α:

$$\nu_5/\nu'_5 = ((\mu_{Co} + \mu_O)/ (\mu_{Co} + \mu_{O'}))^{1/2} \quad (2)$$

and amounts to 1.0469, when neglecting anharmonicity. Taking the neon values, which are more precise, the corresponding experimental values are 1.0462 for the 469 cm^{-1} band, and 1.0459 for the 685 cm^{-1} one. Assignment of the 469 cm^{-1} band to the B_{2u} motion (displacement of the O atoms parallel to the Co–Co *y* axis) thus appears more likely. Using eqn. (1) yields an estimate value $\alpha = 93°$, and thus 87° for the CoOCo apex angle. The main error source here is the neglect of anharmonicity, which could change from one vibration to the next. Arguments developed below will show that anharmonicity effects seem to be small in this case.

Second, as noted before, each mode of Co_2O_2 isolated in neon shows a specific site pattern. For the ν_4 mode remaining alone in its symmetry class, all components of the isotopic triplet have the same site splitting (Fig. 7a). For the in-plane motions, the site pattern changes with the symmetry of the vibrational mode. Indeed, when looking at the isotopic multiplets around 680 and 460 cm^{-1} for the other fundamentals (Figs. 5–7), it appears clearly that the $Co_2{}^{16}O^{18}O$ central components and the newly activated bands show similar site patterns within the multiplets but for the ν_5 and ν_6 regions. Likewise, the two absorption bands corresponding to the vibrational modes of the $Co_2{}^{16}O_2$ and $Co_2{}^{18}O_2$ molecules are of the same symmetry and have the same site pattern, slightly different from that of the $Co_2{}^{16}O^{18}O$ components. A possible explanation for this phenomenon is the difference in vibrational amplitudes in the nuclear displacements perpendicular or parallel to the molecular axis, inducing slightly different frequency shifts according to the strength of the guest–host interaction in low symmetry trapping sites. As the symmetry is reduced in $Co_2{}^{16}O^{18}O$, the normal modes differ and the observed pattern due to matrix site splitting also changes. These differences in matrix perturbation will prove helpful in assigning weak combinations and confirming the vibrational assignments. Considering the weak 917 and 867 cm^{-1} combination bands, these show the same profile as the 685 cm^{-1} fundamental (Fig. 5) and are thus likely to be of the same symmetry. With D_{2h}, an IR-active binary level is neither an overtone nor a combination of two IR active fundamentals, so it must involve the combination of an IR active motion and an A_g or B_{1g} mode. From the $Co_2{}^{16}O^{18}O$ data, we know that two A_g and B_{1g} fundamentals come around 710 and 460 cm^{-1}. Given the positions of the known fundamentals, no good match is found for the 867 cm^{-1} band, except supposing a combination of the remaining A_g mode with the 685 cm^{-1} one, placing the former around 183 cm^{-1}. The 917 cm^{-1} combination is then likely to arise from the *ungerade* mode at 469 and the *gerade* one near 460 cm^{-1}, which is confirmed by observation of a weak band at 899.9 with $Co_2{}^{16}O^{18}O$. Supposing assignment of the upper modes near 710 and 685 to B_{1g} and B_{2u} vibrations in $Co_2{}^{16}O_2$, would lead to assignments of the 467 and 460 bands to B_{3u} and A_g vibrations, but a combination of these latter two would be of B_{3u} symmetry, different from that of the 685 cm^{-1} band. Reversing the assignments leads, however, to a self-consistent picture, with $2A_g$ and B_{3u} for 710, 183 and 685 cm^{-1} fundamentals, B_{2u} and B_{1g} for the 467 and 460 cm^{-1} ones, giving B_{3u} symmetries for both the 917 and 867 cm^{-1} combinations ($B_{1g} \otimes B_{2u} = B_{3u}$ and $A_g \otimes B_{3u} = B_{3u}$).

In order to check the consistency of our vibrational and structural hypotheses and give quantitative estimates for the Co–O bond force constant, calculations of frequencies and isotope effects have been performed fitting the seven independent potential constants of an harmonic potential on the 18 isotopic frequencies, and results are presented in Table 3. If all frequencies are reproduced within at most two wavenumbers, the reproduction of the isotope effects is much better (within 0.5 cm^{-1}). Subsequently, some anharmonic constants can be estimated, such as X_{16} and X_{35}, with quite small values of the order of −3 and −8 cm^{-1}, respectively. Also, for a D_{2h} symmetry ring molecule and in the electrical and mechanical harmonic approximation, the relative IR intensities can be modeled for all in-plane vibrations using a two electro-optical parameter set ($\partial\mu_x/\partial R_i$ and $\partial\mu_y/\partial R_i$, with $\mu_{x,y}$ being the dipole moment components along the cartesian axes, and R_i, i = 1–4 for the four Co–O coordinates). Taking the eigenvectors from the force field calculation and $\partial\mu_x/\partial R_i = 1.22\ \partial\mu_y/\partial R_i$ will reproduce the observed relative intensities for $Co_2{}^{16}O_2$ and predict those reported in Table 3 for the five in-plane motions of $Co_2{}^{16}O^{18}O$. The most intense four are within experimental error of the observed intensity ratios, and the lowest frequency A_1 mode is predicted with a much smaller relative intensity, consistent with its non-observation.

The bond angle estimate shows a structure close to a square-ring structure, but neglect of the anharmonicity is likely to cause slight deviation from this value. Supposing the same anharmonicity on the B_{3u} mode as that observed for the B_{2u}, one calculates a −2° deviation. It thus seems realistic to state that the CoOCo bond angle value should be within 5° of the 87° estimated value. The Co–O force constant is estimated around 2.43 ± 0.05 N cm^{-1}. Using the Herschbach–Laurie type empirical relationship fitted for diatomic CoO,[12] this would translate in R_{CoO} internuclear distances of 1.765 ± 0.01 Å, which we suggest as a first estimate in the absence of more precise, gas phase data. This would imply a R_{CoCo} distance of the order of 2.55 Å, which might signal a weak remaining metal–metal interaction, in comparison with

Table 3 Comparison of experimental (in neon) and calculated[a] harmonic frequencies (cm^{-1}) for ground state, rhombic Co_2O_2. IR relative intensities are in parenthesis

	Experimental	Calculated	Assignment
	708 ± 5 (0)[b]	710.7 (0)	A_g (ν_1)
	183 ± 5 (0)[b]	182.8 (0)	A_g (ν_2)
$Co_2{}^{16}O_2$	460 ± 5 (0)[b]	458.3 (0)	B_{1g} (ν_3)
	684.5 (1.00)[c]	682.7 (1.00)	B_{3u} (ν_6)
	467.1 (0.67)	466.5(0.67)	B_{2u} (ν_5)
	293.4 (0.24)	293.6	B_{1u} (ν_4)
	671 ± 5 (0)[b]	677.2	A_g (ν_1)
	178 ± 5 (0)[b]	180	A_g (ν_2)
$Co_2{}^{18}O_2$	433 ± 5 (0)[b]	437.8	B_{1g} (ν_3)
	654.4	652.1	B_{3u} (ν_6)
	446.5	445.6	B_{2u} (ν_5)
	280.5	280.5	B_{1u} (ν_4)
	702.2 (0.23)	701.5 (0.25)	A_1 (ν_1)
	180 ± 5 (0)[b]	181.5 (3 10^{-6})	A_1 (ν_2)
$Co_2{}^{16}O^{18}O$	437.7 (0.18)	440.9 (0.25)	B_1 (ν_3)
	660.4 (1.00)[c]	659.9 (1.00)	A_1 (ν_6)
	461.8 (0.69)	463.2 (0.59)	B_1 (ν_5)
	287.1 (0.20)	287.1	B_2 (ν_4)

[a] Force constants for Co_2O_2: (N cm^{-1}) $F_{1,1}$ = 2.435; $F_{1,2}$ = 0.176; $F_{1,3}$ = 0.85; $F_{1,4}$ = 0.148; (N cm rad^{-2}) $F_{5,5}$ = 0.71; $F_{5,6}$ = −0.09; $F_{7,7}$ = 1.039. 1 to 4 = CoO coordinates, 5 and 6 = $\theta_{5,6}$ bond angles (see Fig. 10), 7 = OCoOCo dihedral angle. Relative IR intensities calculated for the in-plane vibrations with two electro-optical parameters: $\partial\mu_x/\partial R_{CoO} = 1.22\ \partial\mu_y/\partial R_{CoO}$. [b] Estimated from combination bands. [c] IR relative intensities are measured with an estimated ±20% uncertainty with respect to the strongest band.

neighbouring species (2.154 Å for Ni_2,[19] and close values for other TM dimers[20]).

DFT calculations in ref. 9 for Co_2O_2 do not compare very well with the frequencies, intensities and estimated geometry for the lowest energy state considered (^7A_u), optimized with CoOCo angles of 78° and a shorter Co–Co distance. The ground state of Co_2 is thought to be a quintet[21] and, with the triplet ground state of O_2, the system hence first interacts on the septet surface. From the absence of reaction between ground state Co_2 and O_2 reagents observed here, it seems unlikely that the observed ground state of Co_2O_2 corresponds to a state accessible directly within the septet surface. The frequencies calculated for one of the quintet states ($^5B_{1g}$), 27 kcal mol^{-1} above the ^7A_u state, are in better agreement with the spectroscopic data, but clearly more work needs to be carried out at a higher level, and states with lower spin multiplicity should also be considered in future work.

Structures of metastable states Co_2O_2–a and Co_2O_2–b

The data obtained for the metastable states formed after electronic excitation of Co_2O_2–X are far less complete than for the stable, ring-shaped structure. Nevertheless, many indications can be gained from the analysis of vibrational data. For both states, the results obtained with the $^{16}O^{18}O$ isotopic precursor unambiguously show twice the number of vibrational bands as when using either $^{16}O_2$ or $^{18}O_2$. This shows that in each structure, two different $Co_2{}^{16}O^{18}O$ isotopomers exist and that the two O atoms are no longer equivalent.

Co_2O_2–a. This state is characterized by four fundamental frequencies in argon matrix experiments, only the strongest two were observed in neon. The upper band presents a frequency near 840 cm^{-1}, with a $^{16}O/^{18}O$ isotopic effect very close to that expected for an isolated CoO oscillator at this frequency, not far below that of diatomic CoO. The next two absorptions lie below 550 cm^{-1}, at frequencies typical of bridging oxygen motions. The 545 cm^{-1} band presents a relatively large $^{16}O/^{18}O$ isotopic effect, larger than that for an isolated CoO oscillator, and the next at 530 cm^{-1} is weaker with a slightly smaller effect. The remaining band lies at very low frequency, typical of bond angle deformations.[11] These elements suggest a structure with non equivalent O atoms with one terminal fairly short and strong Co═O bond and a bridging oxygen, such as depicted Fig. 11(a). To check that such a conjecture is realistic, we estimated the isotopic effects which could be calculated with a three-oscillators model, assuming O═Co–O and Co–O–Co′ bond angles of 120° and 90°, respectively. The results obtained for Co═O, Co–O and O–Co′ bond force constants of 4.91, 2.27 and 2.18 N cm^{-1} are presented in Table 4, along with the experimental data. The model quantitatively reproduces the salient points, namely the overall $^{18}O_2/^{16}O_2$ isotopic effects and the small shifts for the ^{18}O═Co–^{16}O–Co and ^{16}O═Co–^{18}O–Co isotopomer frequencies with respect to the ^{16}O═Co–^{16}O–Co and ^{18}O═Co–^{18}O–Co frequencies.

Co_2O_2–b. This state also presents a low symmetry structure, as demonstrated by the existence of two $Co_2{}^{16}O^{18}O$ isotopomers, nevertheless it presents different vibrational characteristics. The upper mode near 985 cm^{-1} presents a broad profile and has a very large $^{16}O_2/^{18}O_2$ isotopic shift, very close to that expected for a O–O isolated oscillator (−54.5 *vs.* −56.3 cm^{-1} at this frequency). The next mode, with a much sharper profile, presents a $^{16}O_2/^{18}O_2$ isotopic effect very close, but yet slightly larger, to that expected for an isolated Co═O oscillator (−42.7 *vs.* −42.0 cm^{-1}). Data obtained with $Co_2{}^{16}O^{18}O$ isotopomers indicate a vibrational coupling between these two coordinates, as for one isotopomer the broad band is shifted to an intermediate position between the $^{16}O_2$ and $^{18}O_2$ positions, while the lower sharp band gives a component shifted upward by about 6 cm^{-1}. For the second $Co_2{}^{16}O^{18}O$ isotopomer, the observation of two bands near 960 and 943 cm^{-1} with closer intensities and line widths is consistent with a stronger coupling. A third band is observed near 551 cm^{-1}, in the region typical of bridging oxygen vibrations. This indicates the existence of a second type of structure with an O–O linkage, one relatively strong Co═O bond and a second bridging Co atom, as suggested on Fig. 11b. To substantiate this second conjecture, harmonic frequencies were calculated using a three-oscillators model of the type Co═O–O–Co, with Co–O–O and Co–O–Co bond angles assumed 120° and 60°, respectively. The calculated isotopic frequencies are compared in Table 5 with our data. This simple model reproduces approximately the important points (total $^{16}O_2/^{18}O_2$ isotopic effects, small coupling between O–O and Co═O oscillators for the Co═^{18}O–^{16}O(Co) isotopomer and stronger coupling for the Co═^{16}O–^{18}O(Co) isotopomer, as the isotope effects then reduce the energy difference between the Co═^{16}O and ^{16}O–^{18}O bond oscillators). Note that this effect is slightly overestimated and a better result would be achieved reducing the Co–O–O bond angle. Given the level of approximation, we are not aiming here at a geometrical estimate, only at defining a range of realistic structures. The magnitude of the O–O bond force constant would be typical for the peroxide bond (4.85 compared to 4.0 N cm^{-1} in H_2O_2[22]) but the Co═O force constant would be remarkably high (5.83 compared to 5.3 N cm^{-1} in CoO), close to the value for the OCoO triatomic molecule.[12]

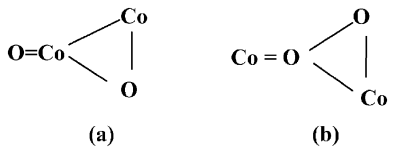

Fig. 11 Proposed schematic structures for metastable states Co_2O_2–a and Co_2O_2–b.

Table 4 Comparison of experimental frequencies[a] for metastable state Co_2O_2–a and calculated[b] harmonic frequencies (cm^{-1}) for a O═Co–O–Co, three-oscillators model (see text and Fig. 11)

	Experimental	Calculated	Approximate description
	839.4	839.8	O═Co
^{16}O═Co–^{16}O–Co	544.8	544.5	Co′–O
	530.0	530.4	Co–O
	805.0	804.8	O═Co
^{18}O═Co–^{18}O–Co	519.1	528.4	Co′–O
	505.7	502.0	Co–O
	806.6	806.6	O═Co
^{18}O═Co–^{16}O–Co	543.0	544.2	Co′–O
	528.3	524.7	Co–O
	838.6	838.1	O═Co
^{16}O═Co–^{18}O–Co	521.3	520.3	Co′–O
	507.8	507.2	Co–O

[a] In solid argon. [b] Force constants (N cm^{-1}) of: $F_{Co=O}$ = 4.915; $F_{O=Co,\ Co-O}$ = −0.3; F_{Co-O} = 2.27; $F_{Co'-O}$ = 2.18, F_{CoCo} = 0.6, O═Co–O and Co–O–Co bond angles assumed 120° and 90°, respectively.

Formation pathway, photo-physics and conclusive remarks

The formation pathway of Co_2O_2 is also of interest. Two separate processes should be discussed: first its formation during sample deposition, and second the reaction within the

Table 5 Comparison of experimental frequencies[a] assigned to metastable state Co_2O_2 –b and calculated[b] harmonic frequencies (cm^{-1}) for a Co═OO(Co), three-oscillators model (see text and Fig. 11)

	Experimental	Calculated	Approximate description
	985.5	986.1	O–O
$Co═^{16}O–^{16}O(Co)$	950.2	951.1	Co═O
	551.5	551.1	Co–O–Co
	931.0	931.0	O–O
$Co═^{18}O–^{18}O(Co)$	907.5	904.6	Co═O
	531.8	528.7	Co–O–Co
	≈960	970.0	(O–O) + (Co═O)
$Co═^{16}O–^{18}O(Co)$	943.5	934.5	(Co═O) + (O–O)
	533.6	530.6	Co–O–Co
	≈948	957.5	O–O
$Co═^{18}O–^{16}O(Co)$	913.9	910.8	Co═O
	550.0	549.0	Co–O–Co

[a] In solid argon. [b] Force constants (N cm^{-1}) of: $F_{Co═O}$ = 5.83; $F_{Co═O,\ O–O}$ = 1.7; $F_{O–O}$ = 4.85; $F_{Co–O}$ = 2.32. Co–O–O and Co–O–Co bond angles assumed 120° and 60°, respectively.

matrix following diffusion at low temperature or photoexcitation of precursors present in the sample. Indeed, the first process cannot be controlled as strictly, since a sizable amount of radiation is emitted by the metal atom source (a grey body at about 1800 K) which cannot be shielded out. The second process (diffusion following annealing to 11 K in neon or 25–30 K in argon) is easier to analyze, as it leads to reactant-pair formation at low temperature and the formation of Co_2O_2 can be followed in absence of any excitation above 700 cm^{-1}, and next in presence of excitation. The formation of Co_2O_2 will be discussed in both cases, and the results for *in situ* formation will be considered first.

Honma and coworkers showed that, in the gas phase, ground state Co (a^4F) does not react with molecular oxygen.[23] It reacts in its first excited state (b^4F, about 3500 cm^{-1} above the ground state). Recent reinvestigations of the reactivity of atomic Co towards molecular oxygen in rare gas matrices confirmed this fact and showed a direct insertion route from the first atomic excited state.[13] In our study using thermally evaporated Co, it also appears that both CoO and Co_2O_2 could be formed during deposition. However, annealing experiments showed that Co_2O_2 was not produced by reaction of ground state reagents (contrary to what is observed for other reactions such as $Co_2 + CO$ [24] or $Ti_2 + N_2$ [25]). There is also a quantity of Co atoms in the matrix constituting a potential reservoir for further reaction. Several reaction pathways could be considered for Co_2O_2 formation:

$$Co^* + O_2 \rightarrow OCoO \text{ and } OCoO + Co^* \rightarrow Co_2O_2 \quad (1)$$

$$2CoO \rightarrow Co_2O_2 \quad (2)$$

$$Co_2 + O_2 \rightarrow Co_2O_2 \quad (3a)$$

$$Co_2^* + O_2 \rightarrow Co_2O_2 \quad (3b)$$

$$Co_2^* + O_2 \rightarrow Co_2O_2^* \quad (3c)$$

Reaction pathway 1 can be ruled out since Co_2O_2 was not formed significantly following Co atom excitation in the first ^4F and ^2F excited states forming OCoO. The second pathway can also be ruled out, because no Co_2O_2 growth was observed at the expense of CoO during annealing. Besides, in $^{16}O_2 + {}^{18}O_2$ experiments where both $Co^{16}O$ and $Co^{18}O$ are present, only $Co_2{}^{16}O_2$ and $Co_2{}^{18}O_2$ were observed and no $Co_2{}^{16}O^{18}O$ was made, indicating clearly an insertion reaction in one oxygen molecule. Pathway 3a seems unlikely since, when annealing the sample directly after deposition without excitation, the quantity of Co_2 remained unchanged. If the Co_2 ground state has the suggested quintet spin multiplicity[21], then both reactants interact first on the septet potential surface. It thus seems that the $Co_2 + O_2 \rightarrow Co_2O_2$ reaction is spin-forbidden, and that ground state of Co_2O_2 has a lower spin state, contrary to the examples given above involving spontaneous reactions of transition metal dimers. This leads us to suspect that Co_2, indeed a precursor, needs to be in an excited state to react with molecular oxygen, as does atomic cobalt.

Co_2O_2 proved to be photosensitive, but could be reformed in larger quantities at the expense of Co_2 only after irradiating in the 540–590 nm range. This can be interpreted as a reaction of O_2 with excited Co_2. Several states were observed for Co_2, precisely in this energy range,[11] broadened presumably by predissociation effects, as these are close to the estimated dissociation energy.[26] The observation of other structures (Co_2O_2–a and Co_2O_2–b) following this process is a strong indication in favor of the bimolecular reaction 3c. The conversion to ground state Co_2O_2–X involves another excitation at lower energy (6000 cm^{-1}), to overcome a small energy barrier. From the energy difference between the two photoexcitations, the metastable states should be between 1.3 and 2 eV above the ground state. Another point concerns the formation pathway of CoO, formed in our experiments only during the sample deposition process in neon, and favored at high deposition temperature. One possibility is that reaction during deposition proceeds on the septet potential surface *via* a Co_2 excited state and, if the excess energy is not quenched rapidly by the rare gas lattice, as expected during the matrix growth in the softer neon medium, dissociation into two CoO molecules ($^4\Delta$ ground state) would proceed to remain on the septet surface. Once the molecule is enclosed in the matrix lattice, electronic excitation only leads to a highly excited state, which relaxes to one of the metastable structures observed (Co_2O_2–a in neon, Co_2O_2–a and Co_2O_2–b in argon), stabilized by the matrix cage. The nature of the electronic metastable states responsible for the two isomers of Co_2O_2 observed here is not clear, and these structures are likely to be influenced by interaction with the matrix, as one is only stabilized in argon. Nevertheless the structures that were discussed above might serve as a guide and we think that, in future theoretical investigations of the Co_2O_2 system, attention should also be paid to high spin states, lying about 1.3 eV above the ground state, and with asymmetrical geometries.

References

1 D. G. Castner, P. Watson and I. Chan, *J. Phys. Chem.*, 1989, **93**, 3188.
2 M. Shirai, T. Inona, H. Onishi, K. Asakura and Y. Iwasawa, *J. Catal.*, 1994, **145**, 159.
3 J. Mackay and V. Henrich, *Phys. Rev. B*, 1989, **39**, 6156.
4 M. M. Natile and A. Glisenti, *Chem. Mater.*, 2002, **14**, 3090.
5 R. B. Freas, B. Waite and J. Campana, *J. Chem. Phys.*, 1987, **86**, 1276.
6 J. J. Klaassen and D. B. Jacobson, *J. Am. Chem. Soc.*, 1988, **110**, 974.
7 A. M. L. Oiestad and E. Uggerud, *Chem. Phys.*, 2000, **262**, 169.
8 A. Martinez, C. Jamorski, G. Medina and D. Salahub, *J. Phys. Chem. A*, **102**, 4643.
9 G. V. Chertihin, A. Citra, L. Andrews and C. W. Bauschlicher, Jr., *J. Phys. Chem. A*, 1997, **101**, 8793.
10 J. Sugar and C. Corliss, *J. Phys. Chem. Ref. Data Suppl. No 2*, 1985, **14**, 513.
11 D. Danset and L. Manceron, *Phys. Chem. Chem. Phys.*, 2004, **6**, 3928.
12 D. Danset and L. Manceron, *J. Phys. Chem. A*, 2003, **107**, 11324.
13 D. Danset, M. E. Alikhani and L. Manceron, *J. Phys. Chem. A*, 2005, **109**, 97; D. Danset, M. E. Alikhani and L. Manceron, *J. Phys. Chem. A*, 2005, **109**, 105.

14 J. G. Dong, Z. Hu, R. Craig, J. R. Lombardi and D. M. Lindsay, *J. Chem. Phys.*, 1994, **101**, 9280.
15 D. M. Mann and H. P. Broida, *J. Chem. Phys.*, 1971, **55** 84.
16 G. A. Ozin and A. J. Hanlan, *Inorg. Chem.*, 1979, **18**, 1781.
17 M. Barnes, D. J. Clouthier, P. G. Hajigeorgiou, G. Huang, C. T. Kingston, A. J. Merer, G. F. Metha, J. R. D. Peers and S. J. Rixon, *J. Mol. Spectrosc.*, 1997, **186**, 374.
18 E. B. Wilson, J. C. Decius and P. C. Cross, *Molecular Vibrations*, McGraw-Hill, New York, 1955.
19 J. C. Pinegar, J. D. Langenberg, C. A. Arrington, E. M. Spain and M. D. Morse, *J. Chem. Phys.*, 1995, **102**, 666.
20 L. J. Jules and J. R. Lombardi, *J. Phys. Chem. A*, 2003, **107**, 1268.
21 C. J. Barden, J. C. Rienstra-Kiracofe and H. F. Schaefer, III, *J. Chem. Phys.*, 2000, **113**, 690.
22 R. Reddington, W. Olson and P. C. Cross, *J. Chem. Phys.*, 1962, **36**, 1371.
23 R. Matsui, K. Senba and K. Honma, *J. Phys. Chem. A*, 1997, **101**, 179.
24 B. Tremblay, L. Manceron, G. L. Gutsev, L. Andrews and H. Partridge, III, *J. Chem. Phys.*, 2002, **117**, 8479.
25 O. Hubner, H. J. Himmel, L. Manceron and W. Klopper, *J. Chem. Phys.*, 2004, **121**, 7195.
26 A. Kant and B. J. Strauss, *J. Chem. Phys.*, 1964, **41**, 3806.